Electronic Supplementary Material (ESI) for New Journal of Chemistry.


**NJ-ART-07-2019-003875 (Revised)**

# Simultaneous formation of non-oxidovanadium(IV) and oxidovanadium(V) complexes incorporating phenol-based hydrazone ligands in aerobic condition

Nirmalendu Biswas, Sachinath Bera, Nayim Sepay, Amrita Pal, Tanmoy Halder, Sudipta Ray, Swarnali Acharyya, Anup Kumar Biswas, Michael G. B. Drew and Tapas Ghosh*

## Electronic Supplementary Information

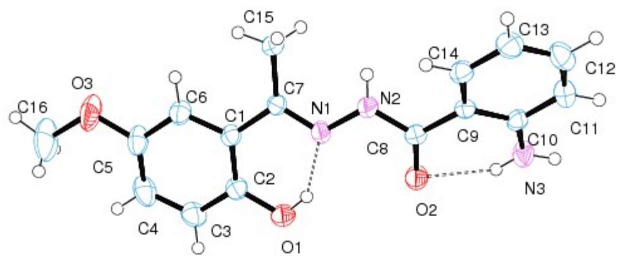


**Fig. S1.** Molecular structure of $H_2L^3$ with ellipsoids at 30% probability. Hydrogen bonds are shown as dotted bonds.

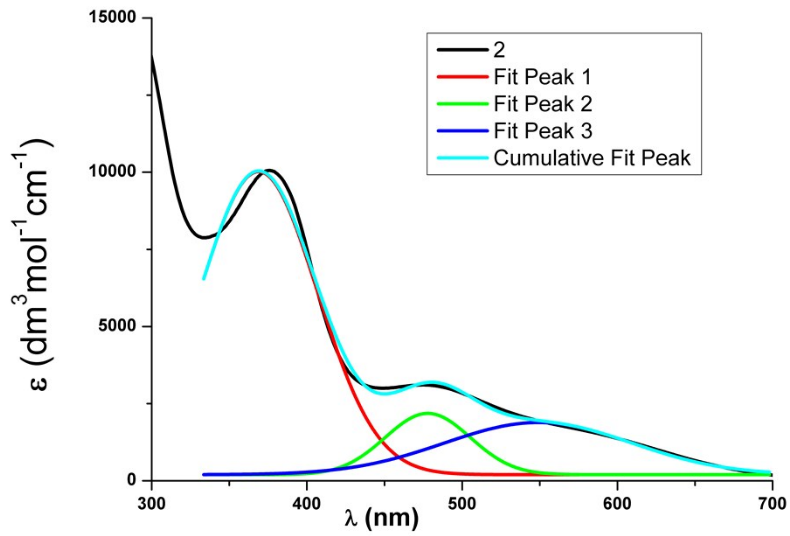


**Fig. S2.** Electronic spectra of **2** in $CH_2Cl_2$. (black experimental; red, green, blue and sky deconvoluted).

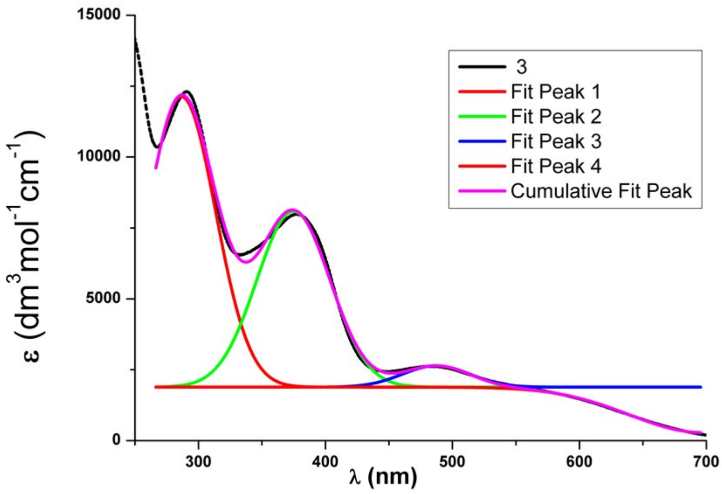


**Fig. S3.** Electronic spectra of **3** in $CH_2Cl_2$. (black experimental; red, green, blue and sky deconvoluted).

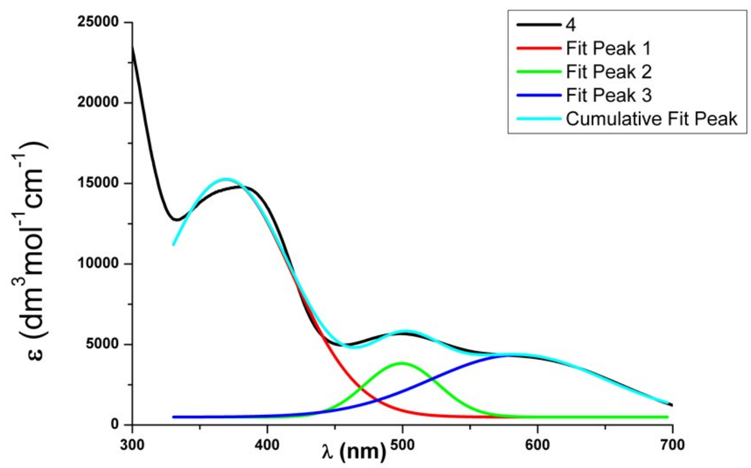


**Fig. S4.** Electronic spectra of **4** in $CH_2Cl_2$. (black experimental; red, green, blue and sky deconvoluted).

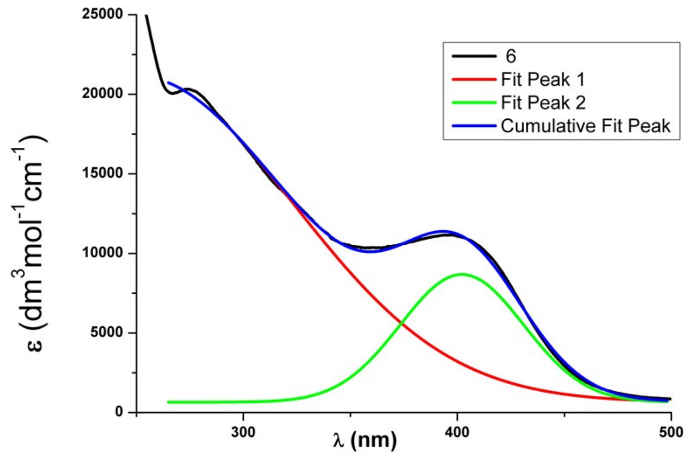


**Fig. S5.** Electronic spectra of **6** in $CH_2Cl_2$. (black experimental; red, green and blue deconvoluted).

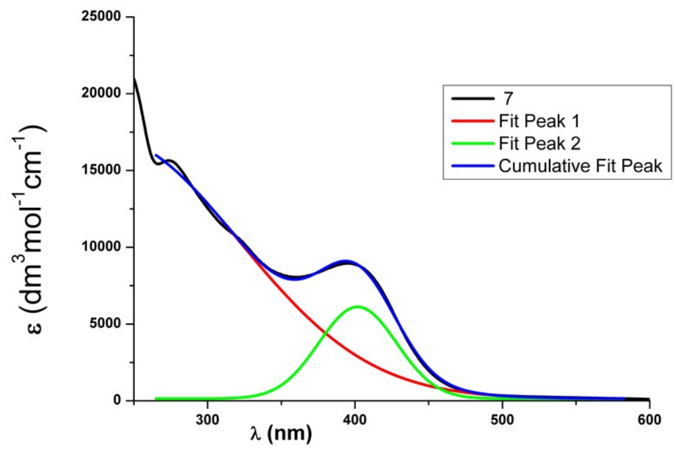


**Fig. S6.** Electronic spectra of **7** in $CH_2Cl_2$. (black experimental; red, green and blue deconvoluted).

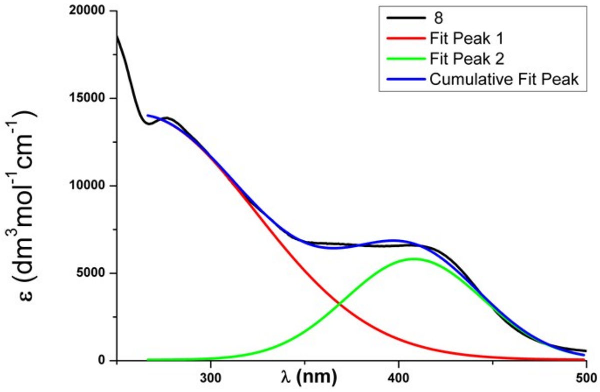


**Fig. S7.** Electronic spectra of **8** in $CH_2Cl_2$. (black experimental; red, green and blue deconvoluted).

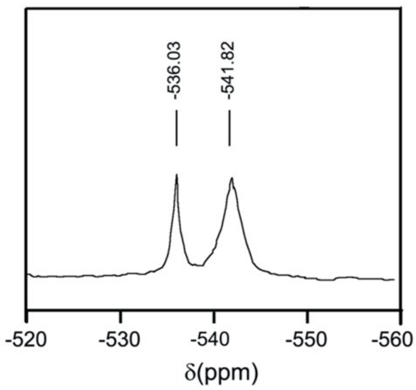


**5**

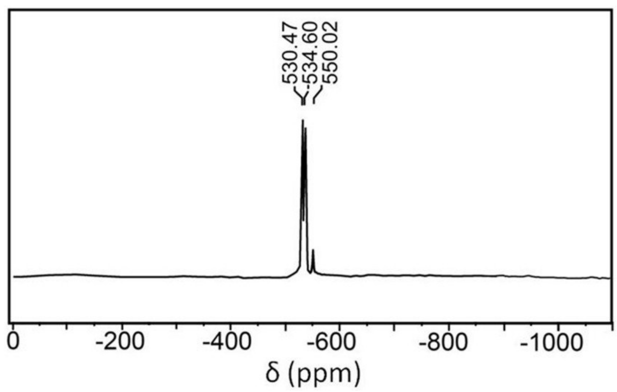


**6**

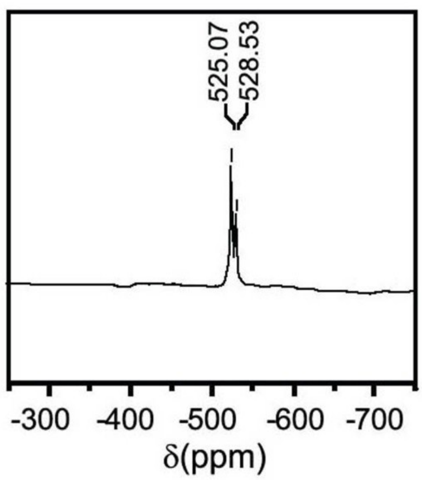


**7**

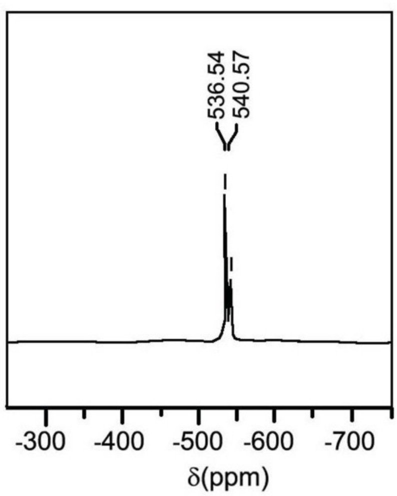


**8**

**Fig. S8**. $^{51}V$ NMR spectra of **5-8** complexes in $CDCl_3$ solution at 298 K.

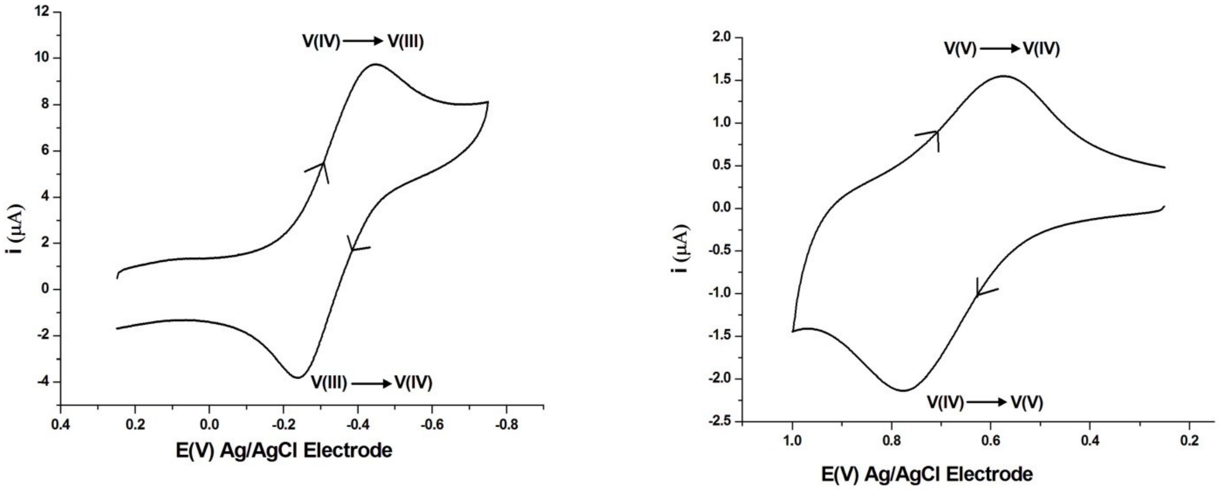


**Fig. S9.** Cyclic voltammogram of **1** in $CH_2Cl_2$.

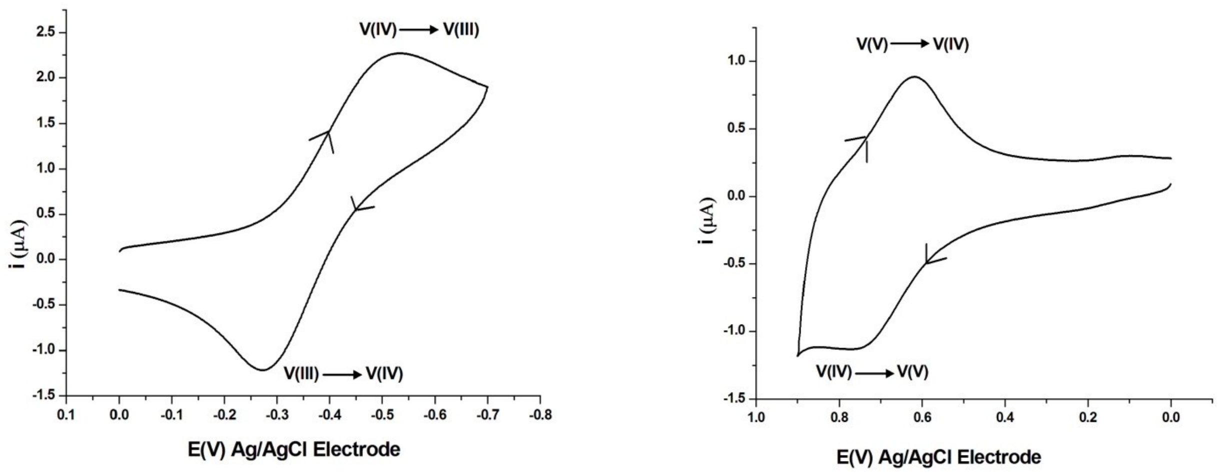


**Fig. S10.** Cyclic voltammogram of **3** in $CH_2Cl_2$.

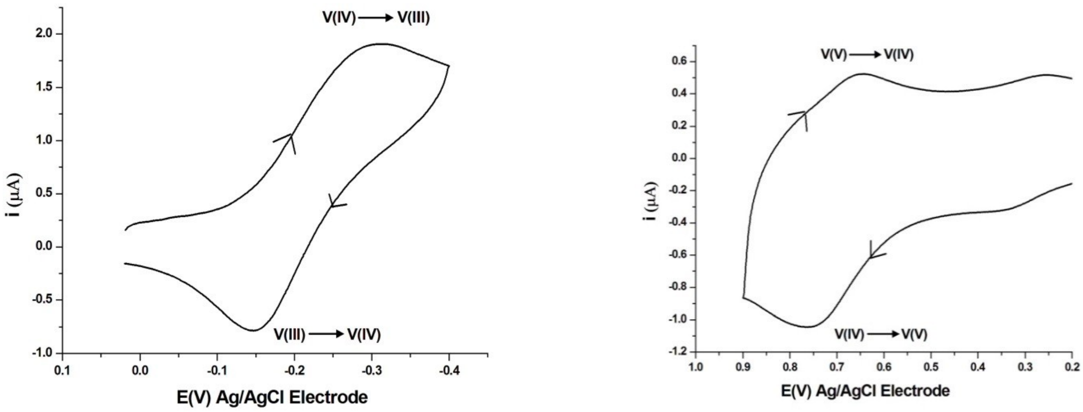


**Fig. S11.** Cyclic voltammogram of **4** in $CH_2Cl_2$.

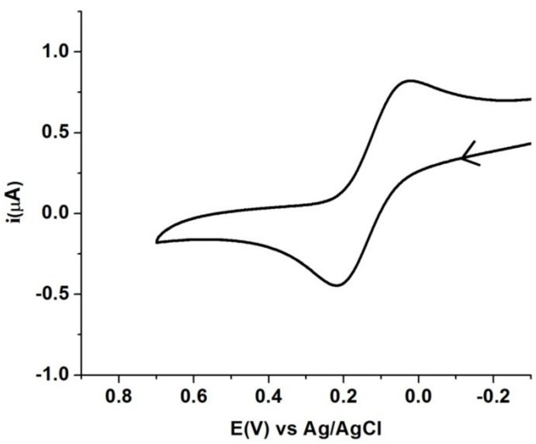


**Fig. S12.** Cyclic voltammogram of **6** in $CH_2Cl_2$.

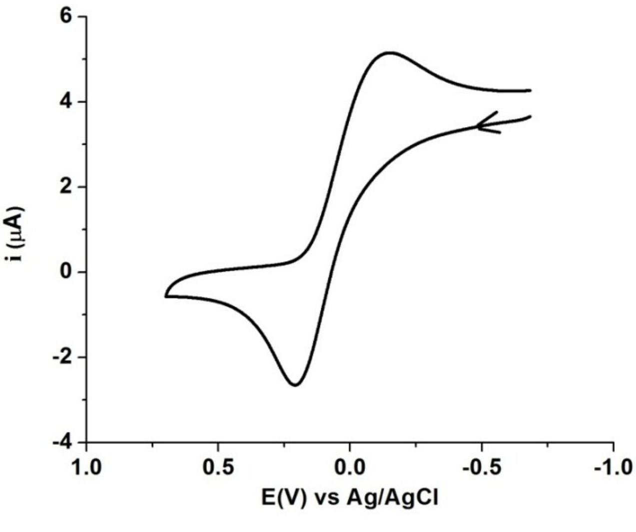


**Fig. S13.** Cyclic voltammogram of **7** in $CH_2Cl_2$.

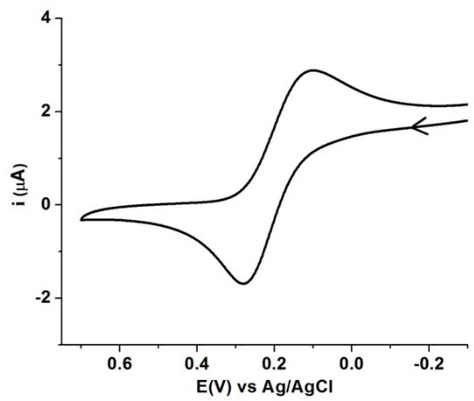


**Fig. S14.** Cyclic voltammogram of **8** in $CH_2Cl_2$.

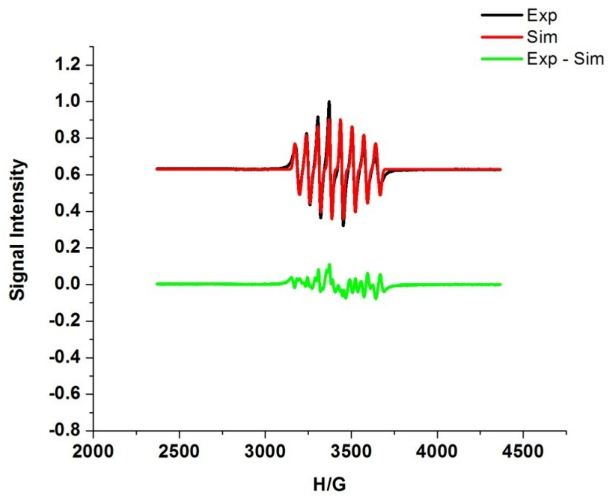


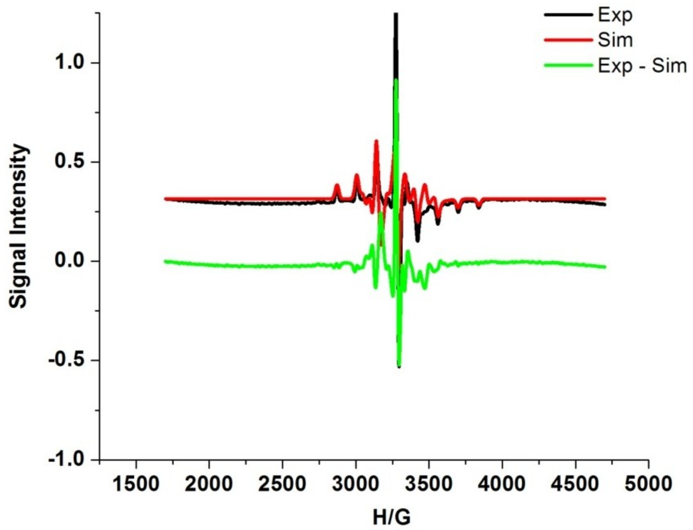


**Fig. S15.** X-band EPR spectra of complex **2** in $CH_2Cl_2$ solution at 300 K (top) and at 77 K (bottom).

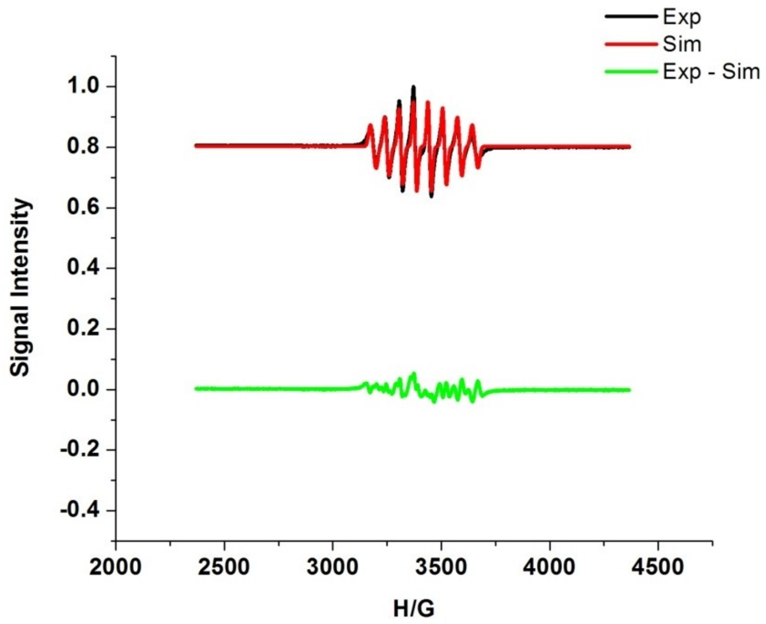


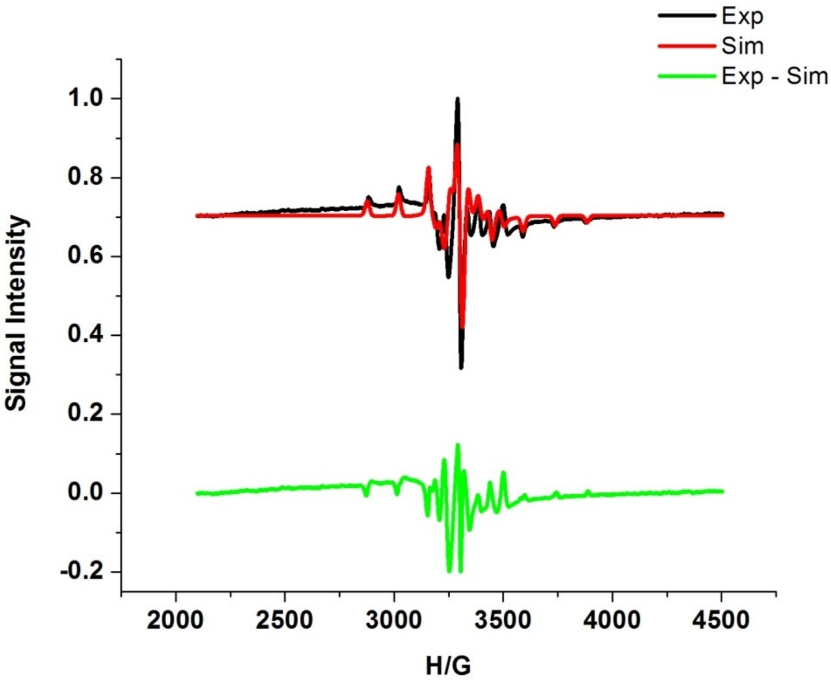


Experimental

on

**Fig. S16.** X-band EPR spectra of complex **3** in $CH_2Cl_2$ solution at 300 K (top) and at 77 K (bottom).

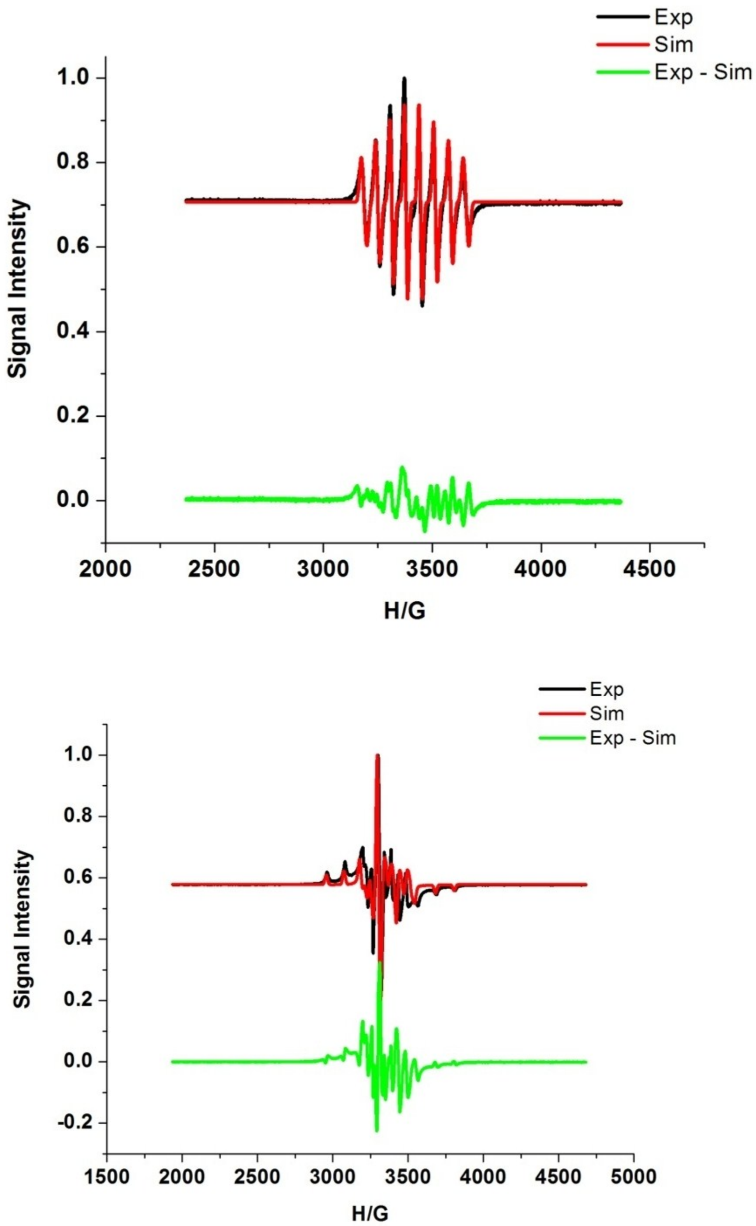


**Fig. S17.** X-band EPR spectra of complex **4** in $CH_2Cl_2$ solution at 300 K (top) and at 77 K (bottom).

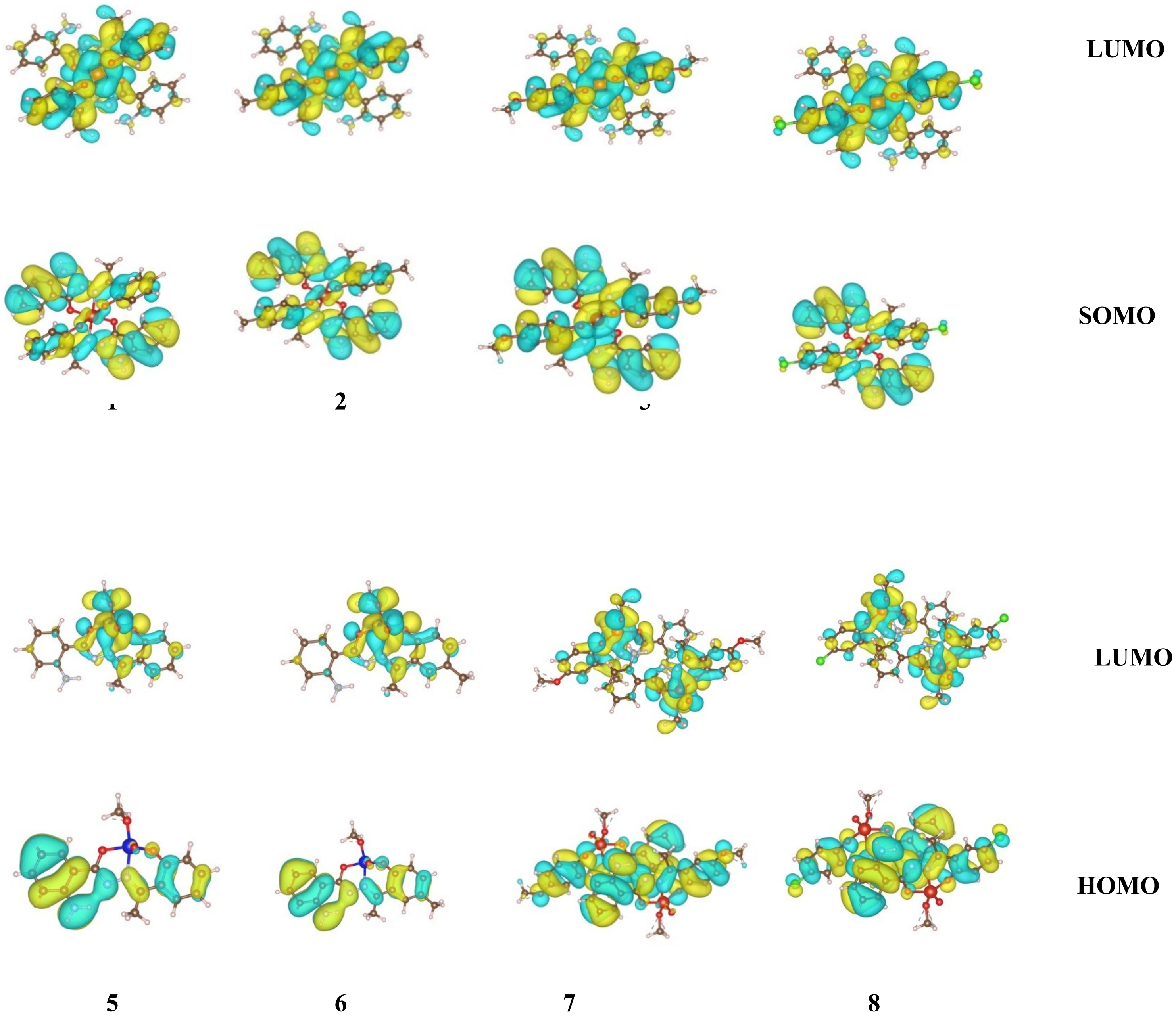


**Fig. S18.** Schematic diagram of selected frontier orbitals of complexes **1-8** in their ground state geometries.

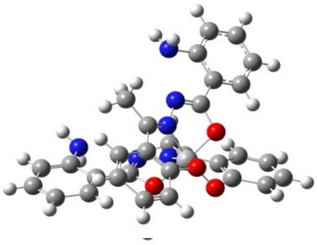

**1**

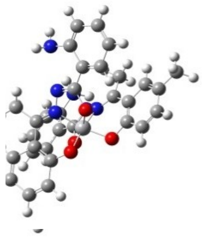

**2**

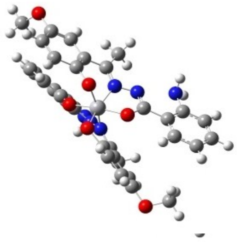

**3**

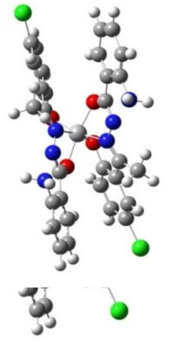

**4**

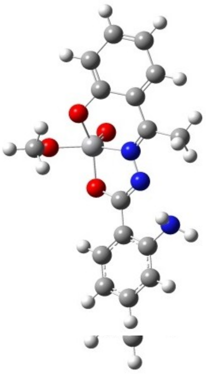

**5**

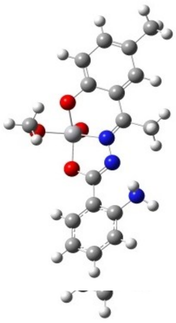

**6**

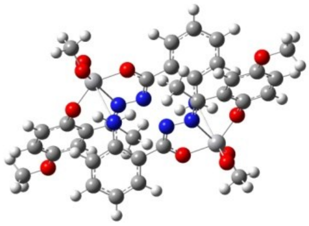

**7**

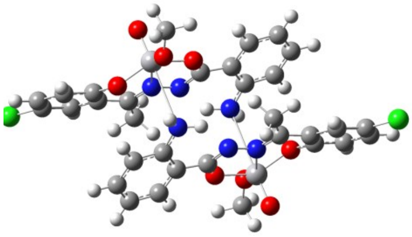

**8**

**Fig. S19.** DFT optimized structure of complexes **1-8.**

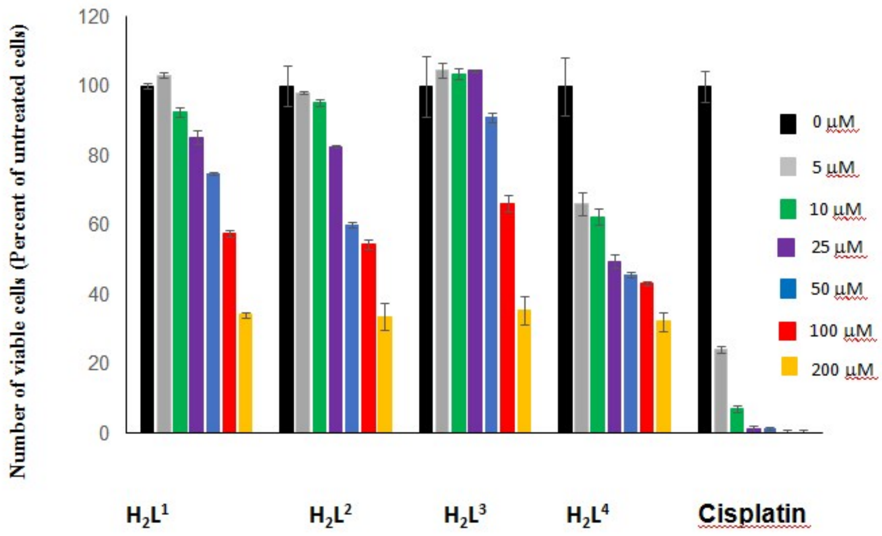


**Fig. S20.** Cytotoxic activity of the $H_2L^{1\text{-}4}$ ligands.

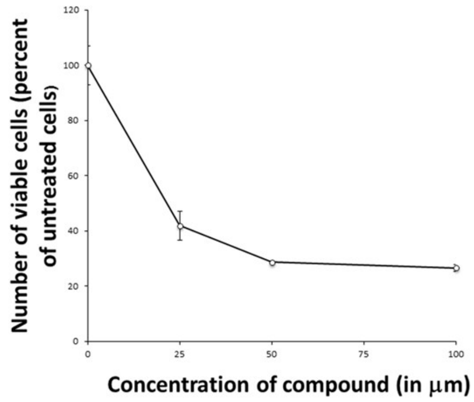


**Fig. S21.** Cytotoxic activity of $[V^{IV}O(aa)_2]$.

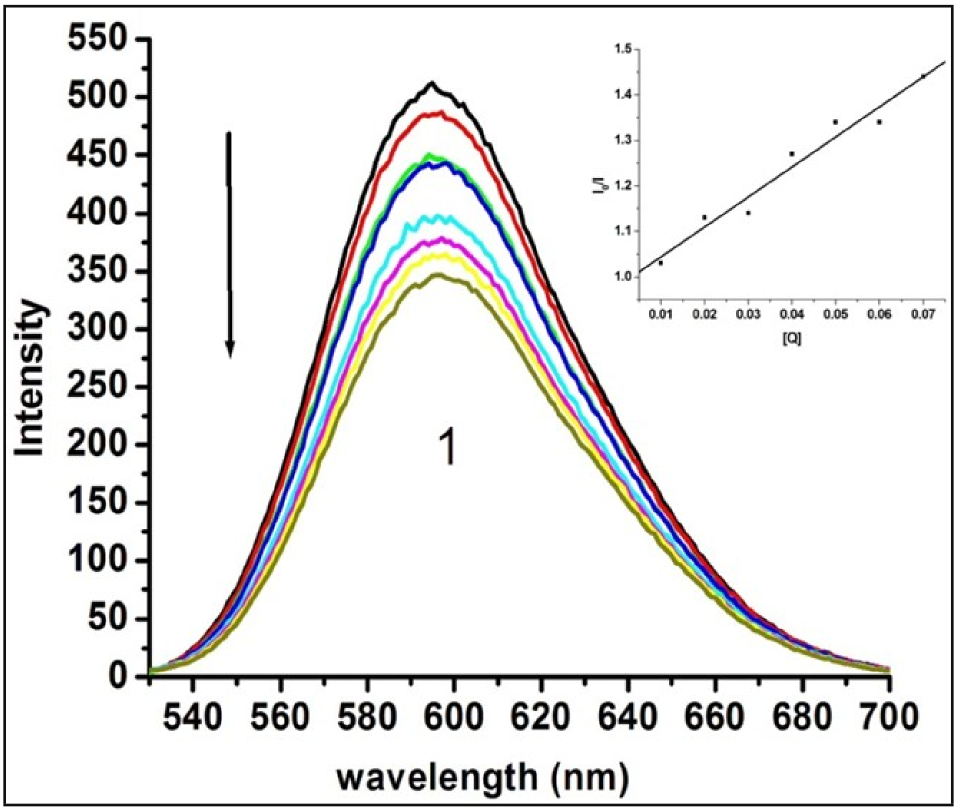


**Fig. S22.** Fluorescence spectra of EB + $10^{-4}$ M DNA control + (1-10) × $10^{-5}$ M complex **1**. The arrow shows that the intensity decreases with increasing concentration of complex 1. (Inset: Stern-Volmer plot for the quenching of fluorescence of the ethidium bromide (EB) - DNA complex caused by complex **1**).

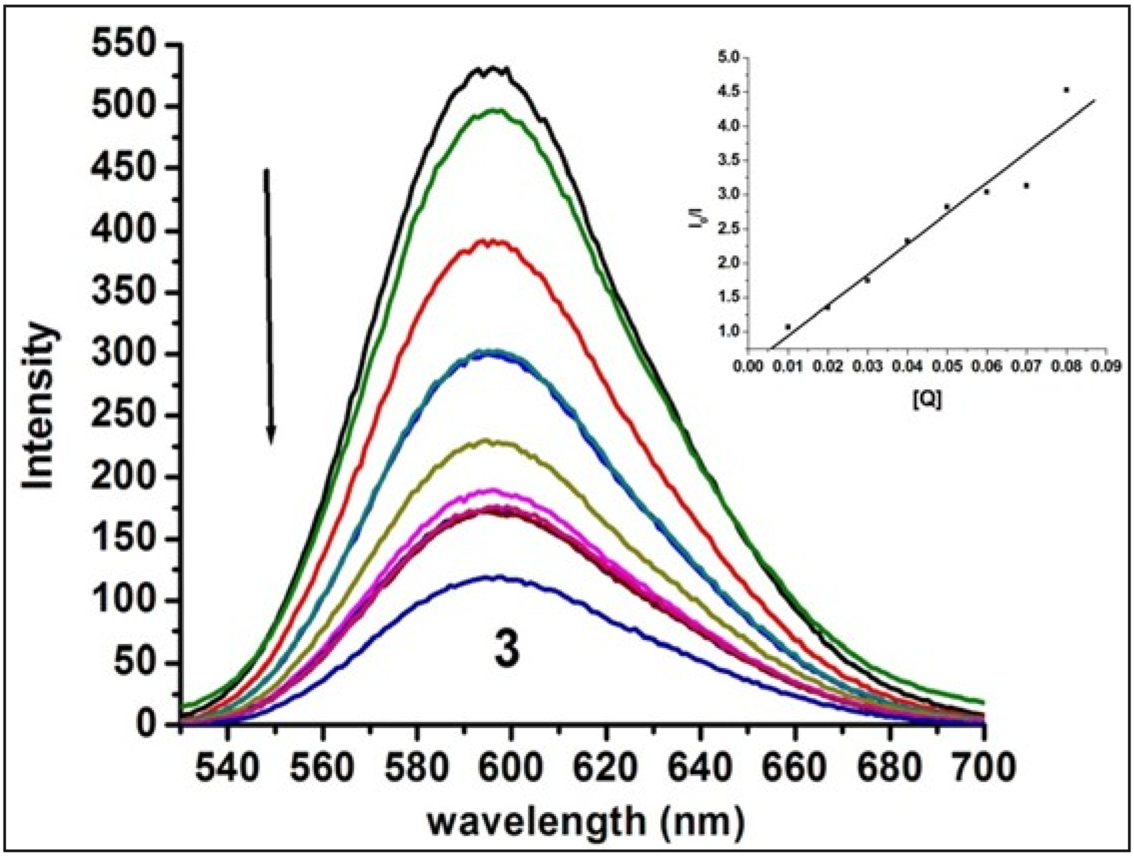


**Fig. S23.** Fluorescence spectra of EB + $10^{-4}$ M DNA control + (1-10) × $10^{-5}$ M complex **3**. The arrow shows that the intensity decreases with increasing concentration of complex 1. (Inset: Stern-Volmer plot for the quenching of fluorescence of the ethidium bromide (EB) - DNA complex caused by complex **3**).

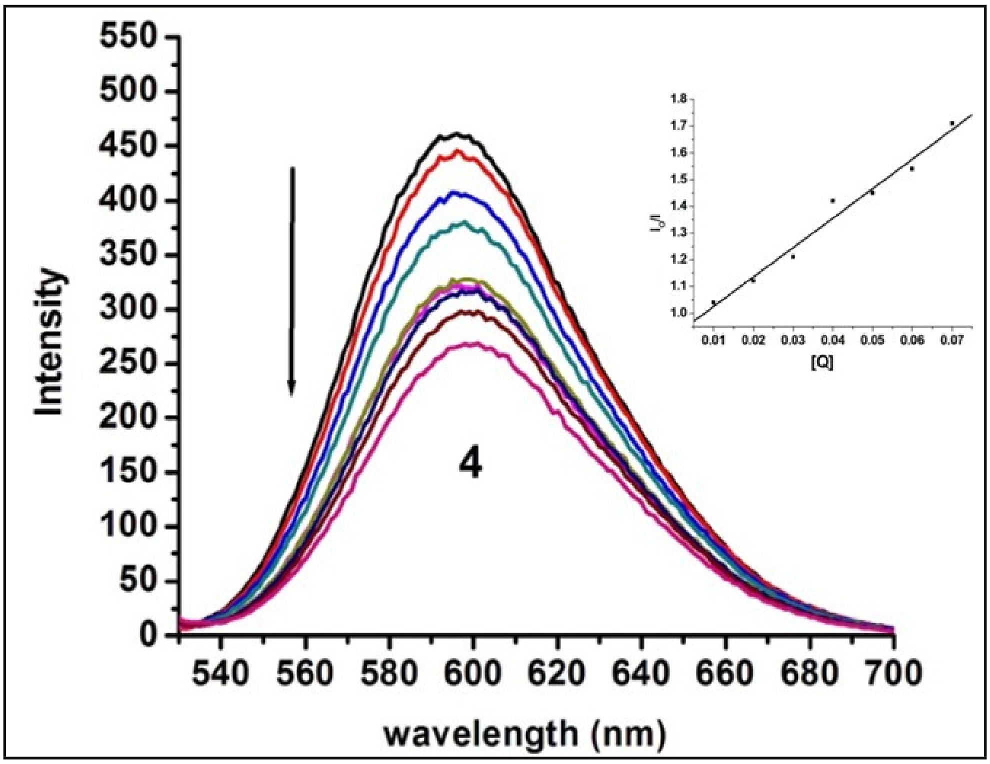


**Fig. S24.** Fluorescence spectra of EB + $10^{-4}$ M DNA control + (1-10) × $10^{-5}$ M complex **4**. The arrow shows that the intensity decreases with increasing concentration of complex 4. (Inset: Stern-Volmer plot for the quenching of fluorescence of the ethidium bromide (EB) - DNA complex caused by complex **4**).

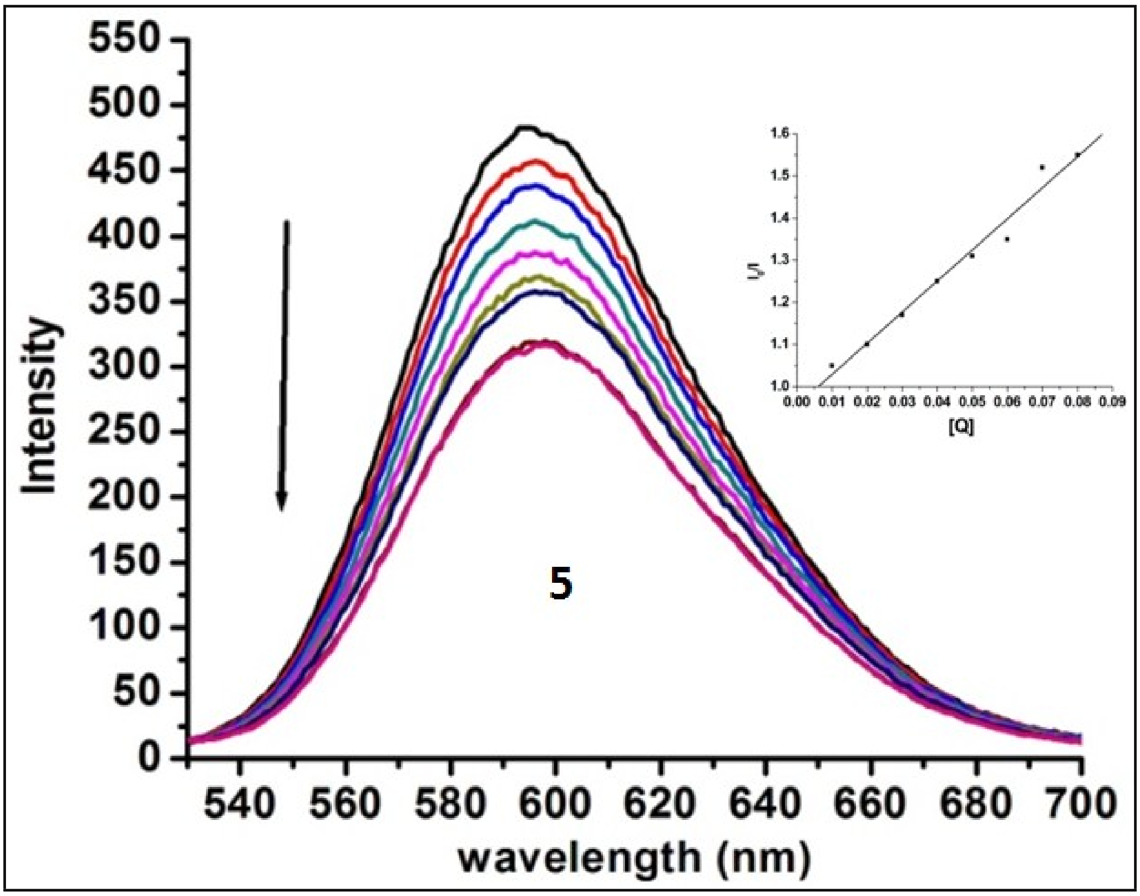


**Fig. S25.** Fluorescence spectra of EB + $10^{-4}$ M DNA control + (1-10) × $10^{-5}$ M complex **5**. The arrow shows that the intensity decreases with increasing concentration of complex 5. (Inset: Stern-Volmer plot for the quenching of fluorescence of the ethidium bromide (EB) - DNA complex caused by complex **5**).

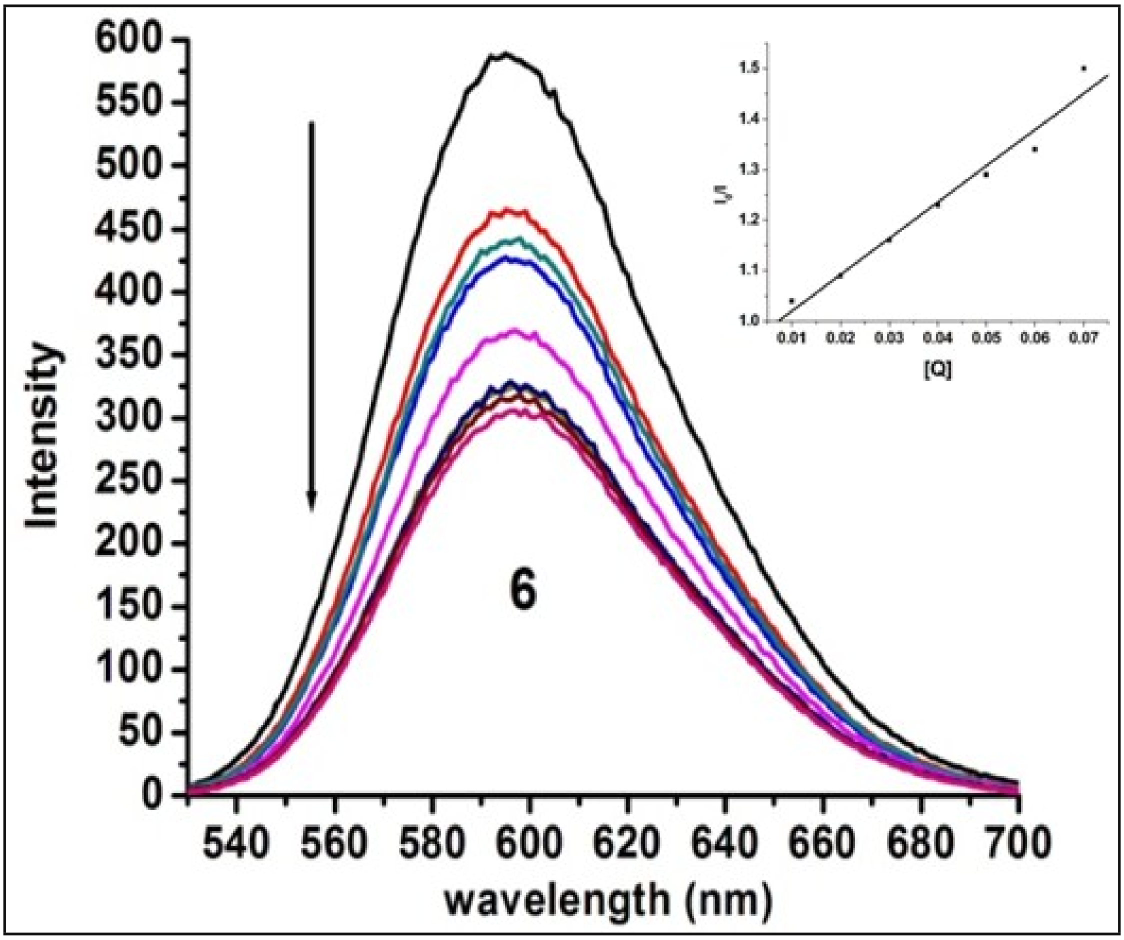


**Fig. S26.** Fluorescence spectra of EB + $10^{-4}$ M DNA control + (1-10) × $10^{-5}$ M complex **6**. The arrow shows that the intensity decreases with increasing concentration of complex 6. (Inset: Stern-Volmer plot for the quenching of fluorescence of the ethidium bromide (EB) - DNA complex caused by complex **6**).

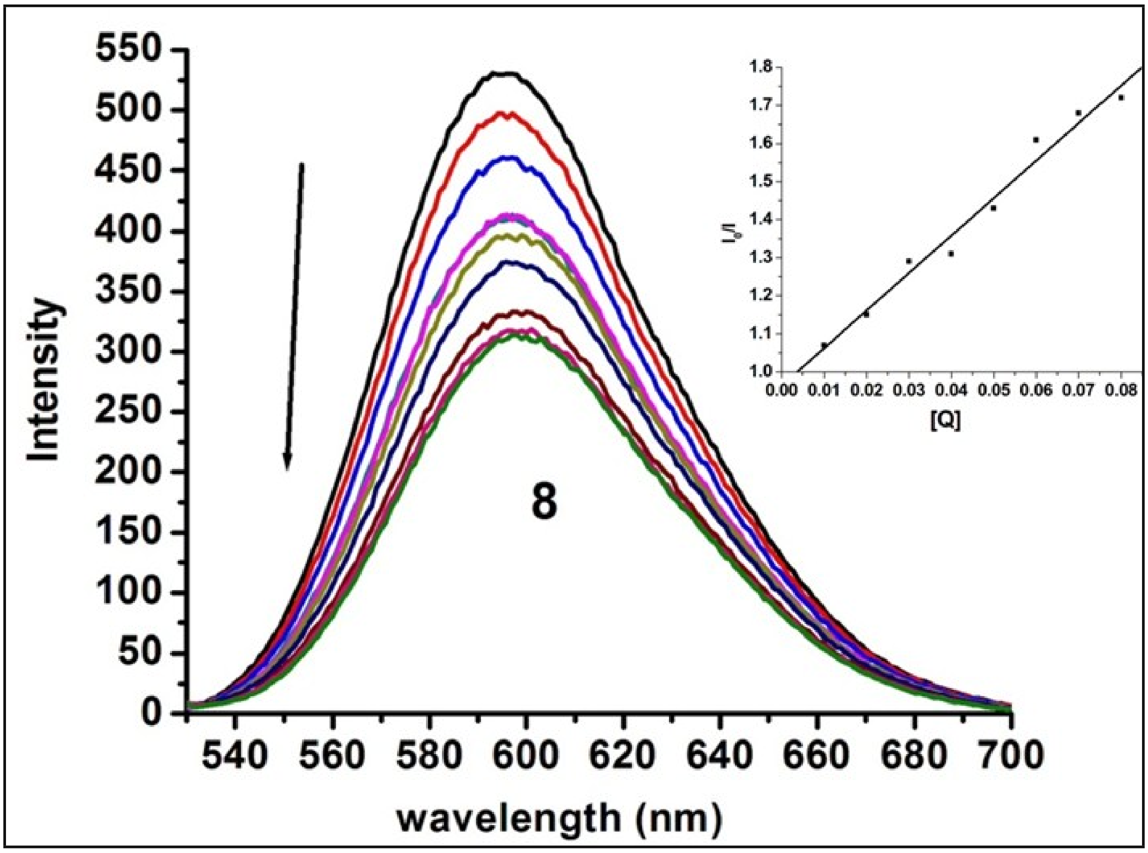


**Fig. S27.** Fluorescence spectra of EB + $10^{-4}$ M DNA control + (1-10) × $10^{-5}$ M complex **8**. The arrow shows that the intensity decreases with increasing concentration of complex 8. (Inset: Stern-Volmer plot for the quenching of fluorescence of the ethidium bromide (EB) - DNA complex caused by complex **8**).

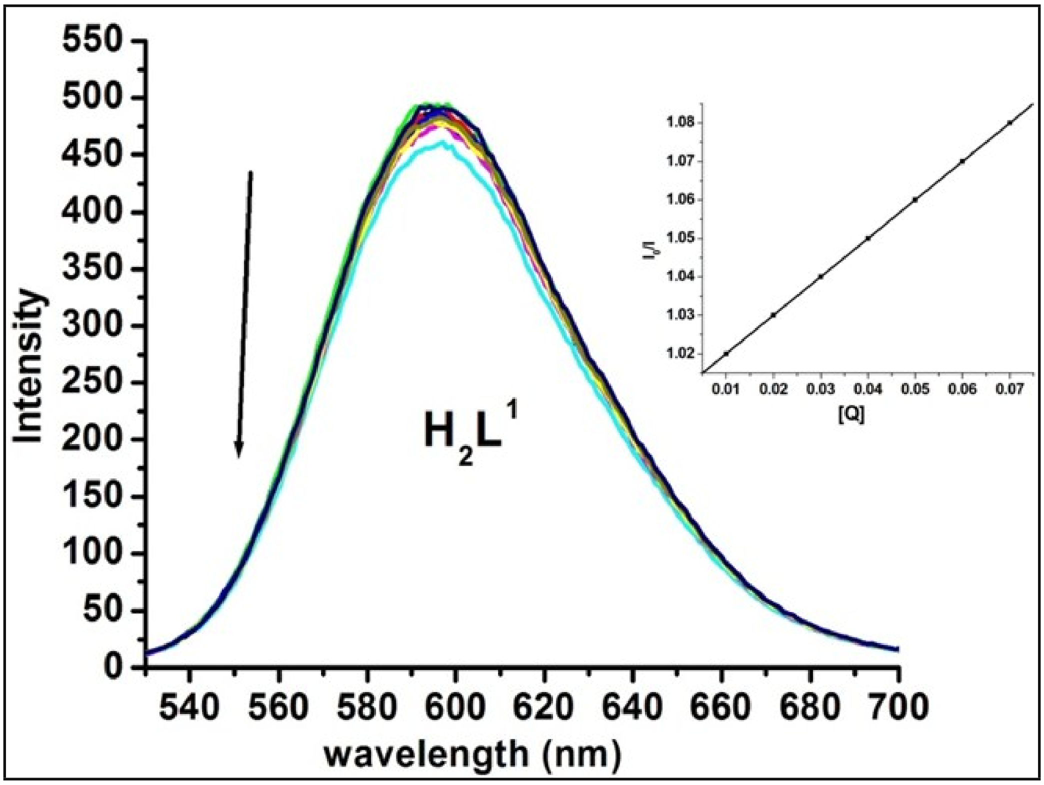


**Fig. S28.** Fluorescence spectra of EB + $10^{-4}$ M DNA control + (1-10) × $10^{-5}$ M ligand $H_2L^1$.The arrow shows that the intensity decreases with increasing concentration of ligand $H_2L^1$. (Inset: Stern-Volmer plot for the quenching of fluorescence of the ethidium bromide (EB) -DNA complex caused by ligand $H_2L^1$).

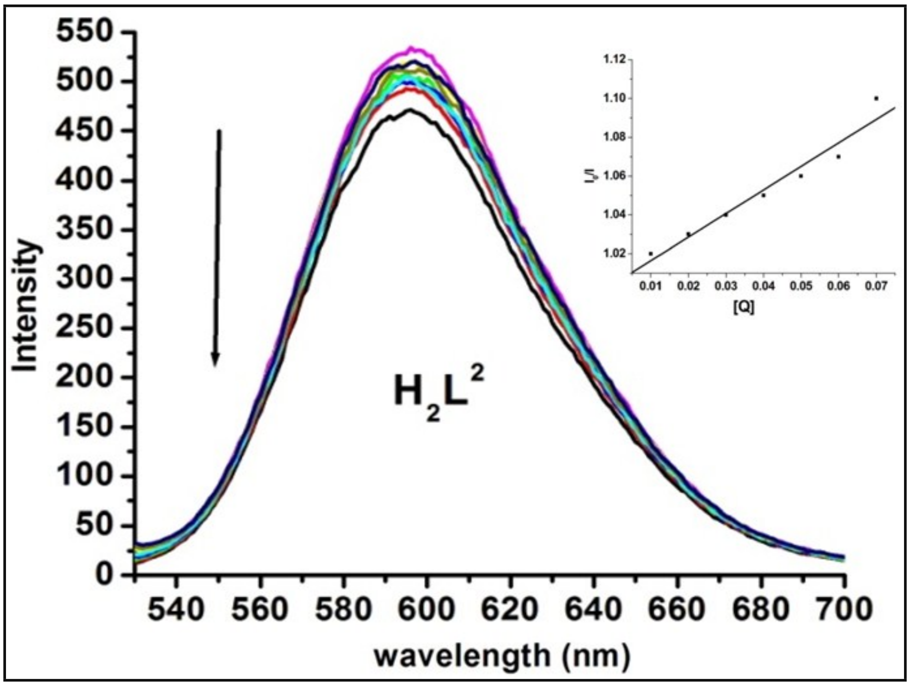


**Fig. S29.** Fluorescence spectra of EB + $10^{-4}$ M DNA control + (1-10) × $10^{-5}$ M complex $H_2L^2$. The arrow shows that the intensity decreases with increasing concentration of ligand $H_2L^2$ (Inset: Stern-Volmer plot for the quenching of fluorescence of the ethidium bromide (EB) -DNA complex caused by ligand $H_2L^2$).

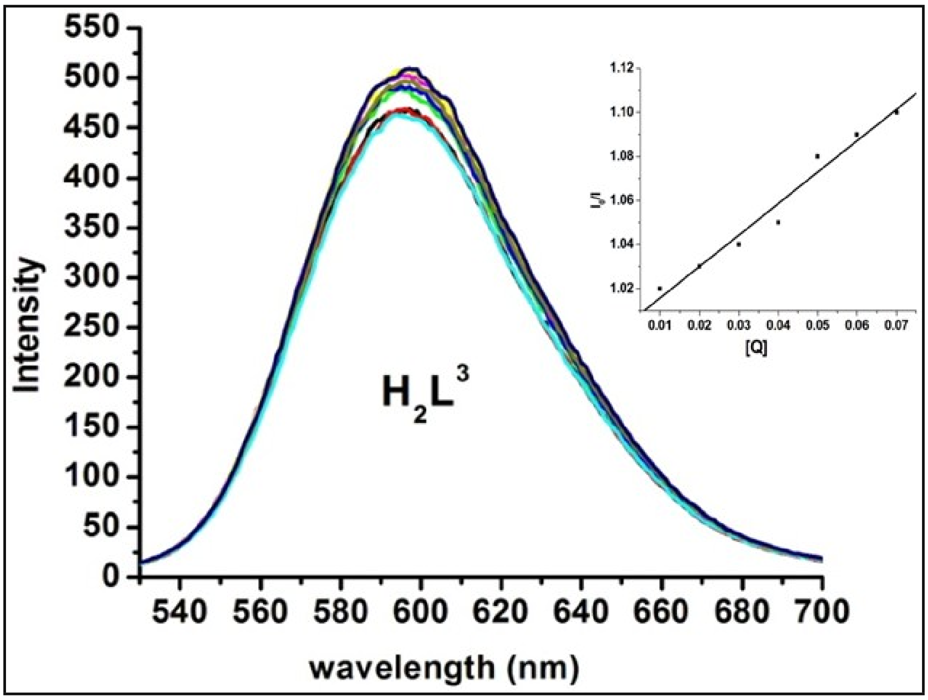


**Fig. S30.** Fluorescence spectra of EB + $10^{-4}$ M DNA control + (1-10) × $10^{-5}$ M complex $H_2L^3$. The arrow shows that the intensity decreases with increasing concentration of ligand $H_2L^3$ (Inset: Stern-Volmer plot for the quenching of fluorescence of the ethidium bromide (EB) -DNA complex caused by ligand $H_2L^3$).

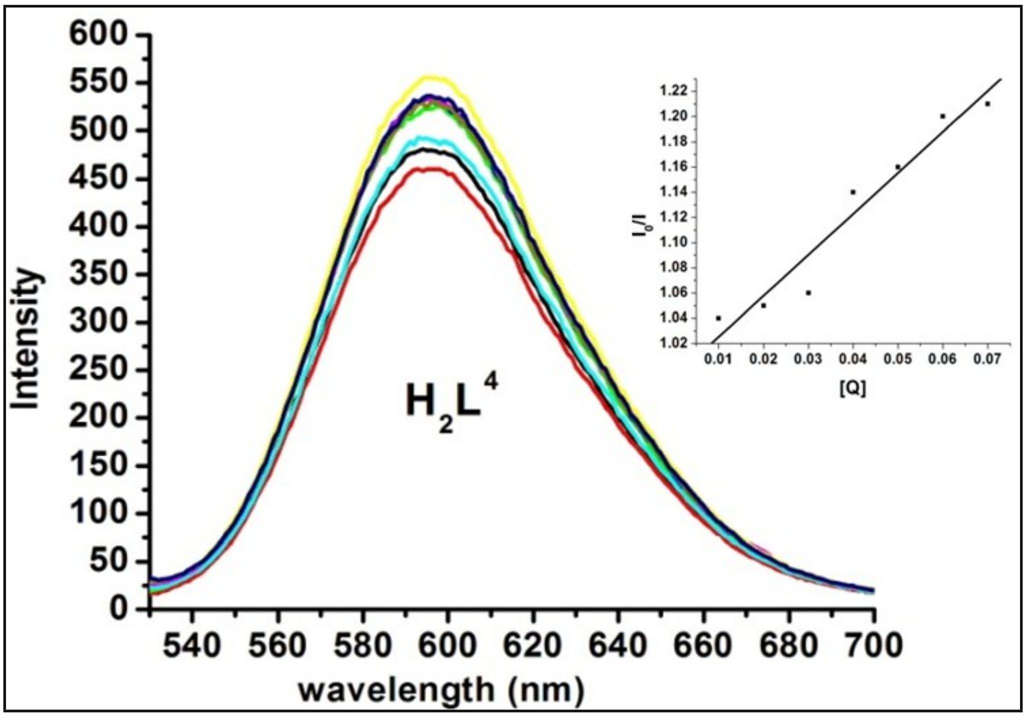


**Fig. S31.** Fluorescence spectra of EB + $10^{-4}$ M DNA control + (1-10) × $10^{-5}$ M complex $H_2L^4$.The arrow shows that the intensity decreases with increasing concentration of ligand $H_2L^4$ (Inset: Stern-Volmer plot for the quenching of fluorescence of the ethidium bromide (EB) -DNA complex caused by ligand $H_2L^4$).

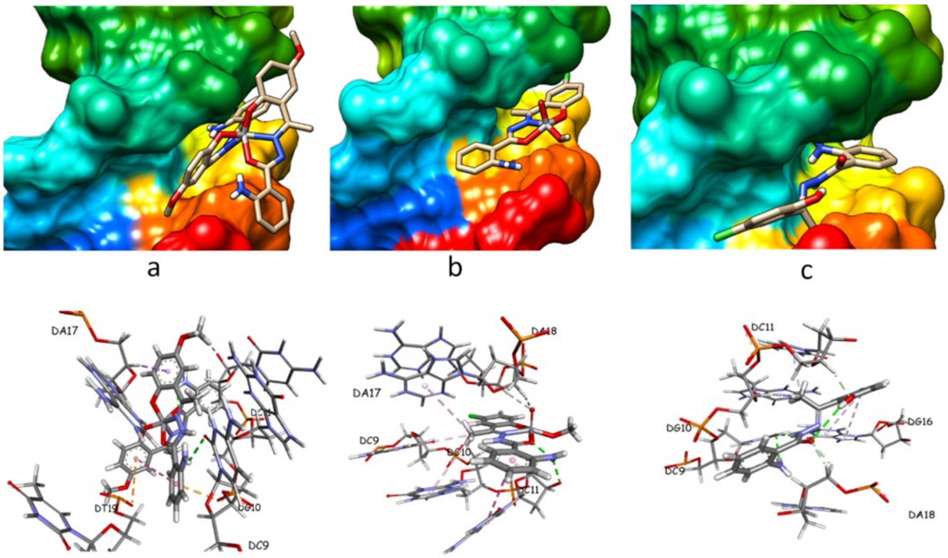


a b c

d e f

**Fig. S32.** Docked pose of complexes **3** (a), **8** (b) and $H_2L^4$ (c) showing interaction with CT DNA base pairs.

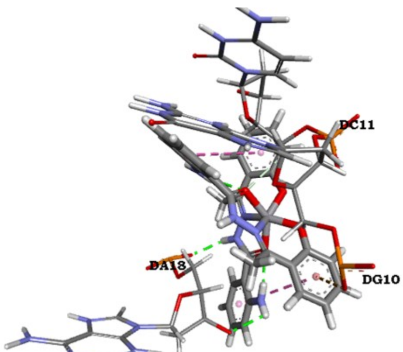


**Fig. S33.** Docked pose of complex **1** showing interaction with CT DNA base pairs.

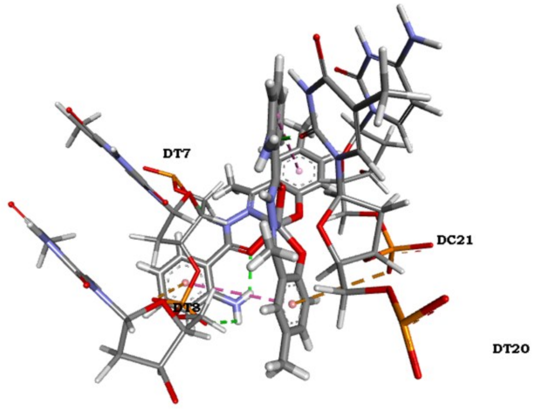


**Fig. S34.** Docked pose of complex **2** showing interaction with CT DNA base pairs.

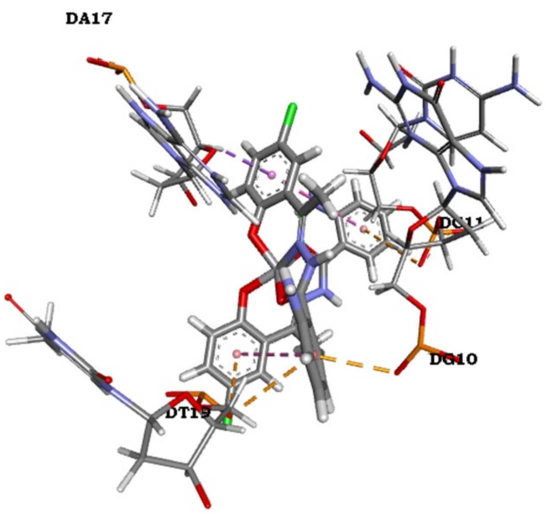


**Fig. S35.** Docked pose of complex **4** showing interaction with CT DNA base pairs.

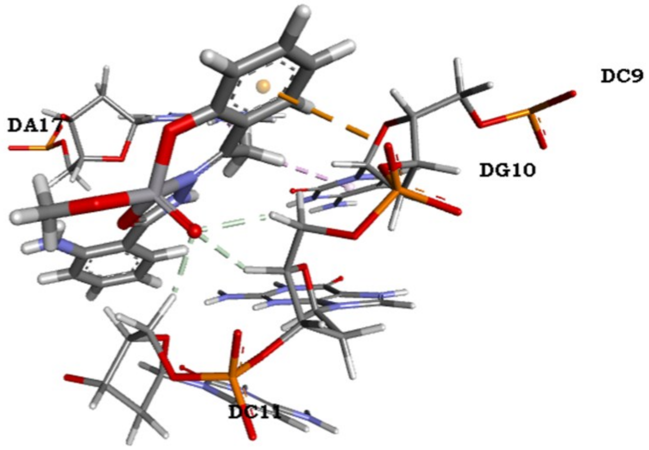


**Fig. S36.** Docked pose of complex **5** showing interaction with CT DNA base pairs.

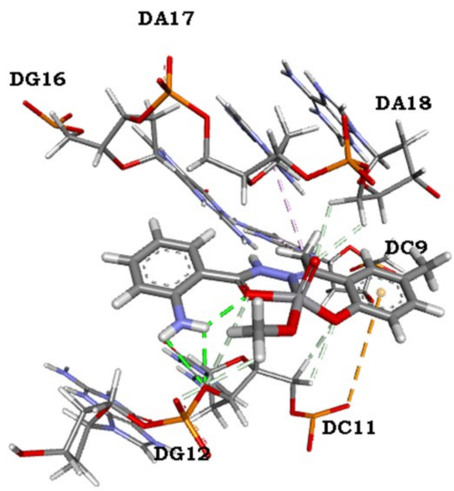


**Fig. S37.** Docked pose of complex **6** showing interaction with CT DNA base pairs.

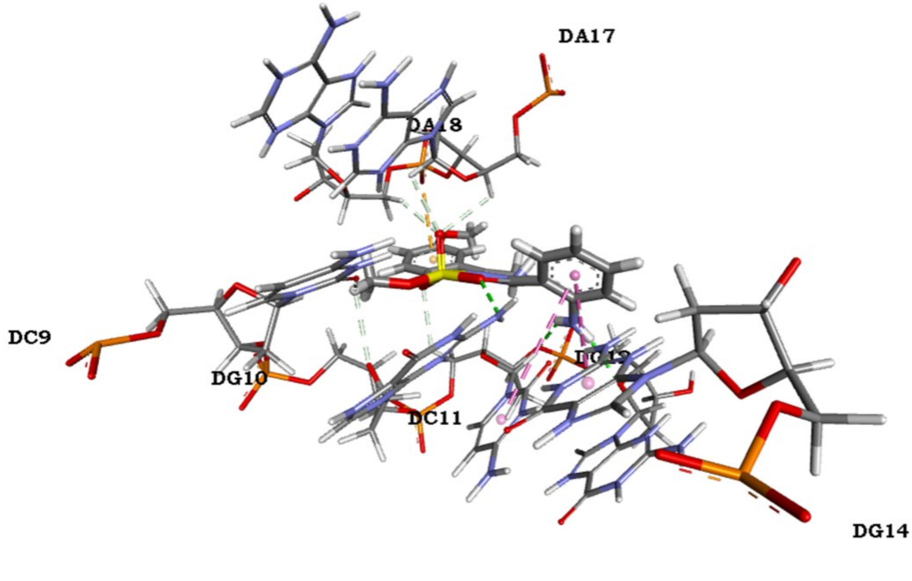


**Fig. S38.** Docked pose of complex **7** showing interaction with CT DNA base pairs.

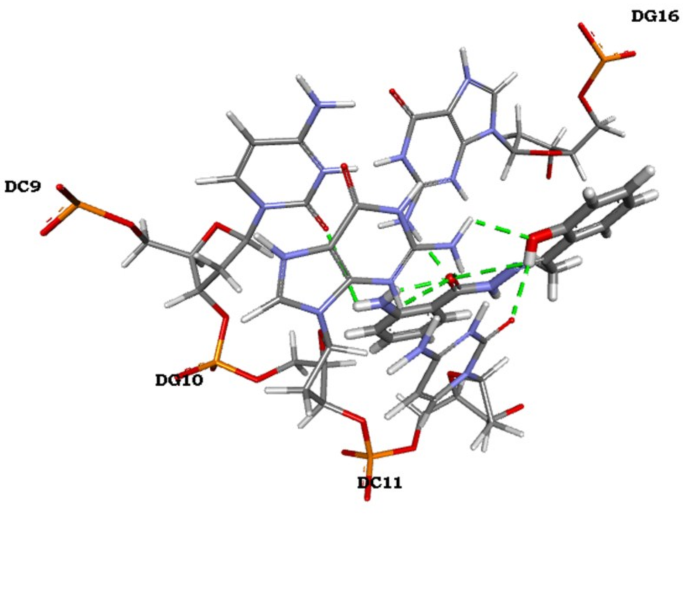


**Fig. S39.** Docked pose of $H_2L^1$ ligand showing interaction with CT DNA base pairs.

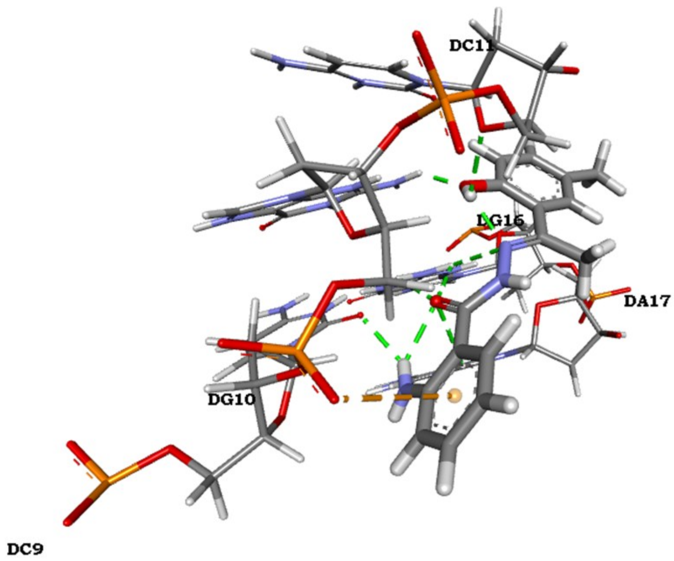


**Fig. S40.** Docked pose of $H_2L^2$ ligand showing interaction with CT DNA base pairs.

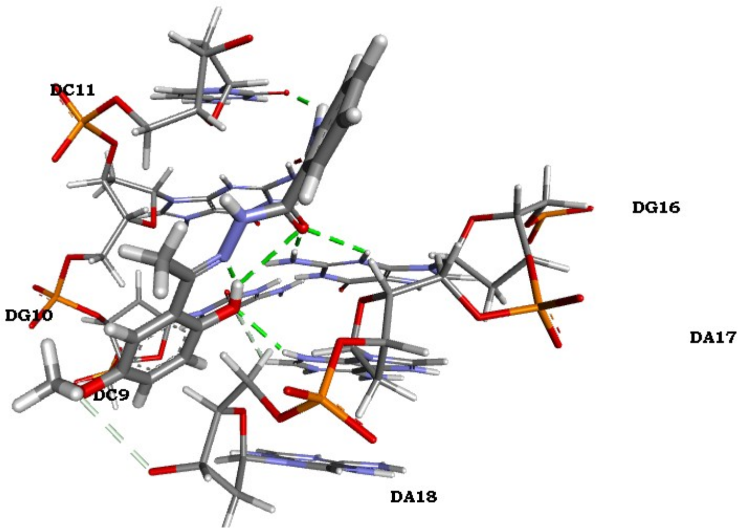


**Fig. S41.** Docked pose of $H_2L^3$ ligand showing interaction with CT DNA base pairs.

Table S1 Dimensions of hydrogen bonds [distances, Å, angles (°)] in ligands $H_2L^2$ and $H_2L^3$.

| D-H…A | d(D-H) | d(H…A) | d(D…A) | <(DHA) | Symmetry element |
|---|---|---|---|---|---|
| | | $H_2L^2$ | | | |
| N3-H3B…O1 | 0.86(2) | 2.25(3) | 3.035(5) | 152(5) | 1-x, -y, -z |
| N3-H3A…O2 | 0.87(2) | 2.08(4) | 2.687(5) | 126(4) | |
| N3-H3A…O2 | 0.87(2) | 2.36(4) | 3.065(5) | 139(4) | 1-x, -y, -z |
| O1-H1…N1 | 0.87(2) | 1.72(3) | 2.522(5) | 152(6) | |
| | | $H_2L^3$ | | | |
| N3-H3B…O1 | 0.87(2) | 2.30(2) | 3.091(3) | 155(3) | -x, -y, 1-z |
| N3-H3B…O2 | 0.87(2) | 2.13(3) | 2.748(2) | 128(3) | |
| N3-H3B…O2 | 0.86(2) | 2.45(3) | 3.127(3) | 134(3) | -x, -y, 1-z |
| O1-H2…N1 | 0.86(2) | 1.74(2) | 2.528(2) | 152(4) | |

Table S2. Dimensions obtained via TD DFT of complexes **1-4**.

| Complex | **1** | **2** | **3** | **4** |
|---|---|---|---|---|
| Bond lengths, Å | | | | |
| V-O1 | 1.888 | 1.887 | 1.885 | 1.889 |
| V-O2 | 1.913 | 1.915 | 1.918 | 1.910 |
| V-N1 | 2.116 | 2.114 | 2.115 | 2.117 |
| Bond angles, deg | | | | |
| O1-V-O2 | 131.15 | 129.62 | 128.12 | 130.83 |
| O1-V-N1 | 81.86 | 81.90 | 81.94 | 81.84 |
| O2-V-N1 | 73.66 | 73.62 | 73.54 | 73.63 |

Table S3. Dimensions obtained via TD DFT of complexes **5**-**8**.

| Complex | **5** | **6** | **7** | **8** |
|---|---|---|---|---|
| bond lengths, Å | | | | |
| V-O1 | 1.843 | 1.842 | 1.833 | 1.844 |
| V-O2 | 1.916 | 1.917 | 1.922 | 1.917 |
| V-O3 | 1.573 | 1.574 | 1.571 | 1.570 |
| V-O4 | 1.771 | 1.772 | 1.775 | 1.772 |
| V-N1 | 2.131 | 2.130 | 2.164 | 2.163 |
| Bond angles, deg | | | | |
| O3-V-O4 | 107.86 | 107.80 | 107.39 | 107.21 |
| O3-V-O1 | 108.18 | 108.32 | 104.68 | 104.19 |
| O4-V-O1 | 97.87 | 97.94 | 98.69 | 98.45 |
| O3-V-O2 | 110.38 | 110.66 | 103.41 | 103.49 |
| O4-V-O2 | 89.17 | 89.14 | 91.98 | 95.52 |
| O1-V-O2 | 136.35 | 135.92 | 145.24 | 145.54 |
| O3-V-N1 | 97.02 | 96.73 | 100.24 | 100.04 |
| O4-V-N1 | 153.75 | 154.07 | 151.22 | 151.76 |
| O1-V-N1 | 81.70 | 81.71 | 81.39 | 81.39 |
| O2-V-N1 | 74.12 | 74.12 | 73.82 | 73.90 |